A Similarity Parameter for Capillary Flows of Relevance to Micropropulsion

Kurt A. Polzin* **and Edgar Y. Choueiri†**
Electric Propulsion and Plasma Dynamics Laboratory (EPPDyL)
Mechanical and Aerospace Engineering Department
Princeton University, Princeton, New Jersey 08544

IEPC-03-64‡

March 17-21, 2003

A similarity parameter for quasi-steady fluid flows advancing into horizontal capillary channels is presented. This parameter, which may be used to scale propellant feeding rates in microthrusters, can be interpreted as the ratio of the average fluid velocity in the capillary channel to a characteristic velocity of quasi-steady capillary flows. It allows collapsing a large data set of previously published and recent measurements spanning five orders of magnitude in the fluid velocity, fourteen different fluids, and four different geometries onto a single curve, and indicates the existence of a universal prescription for such flows. On time scales longer than the characteristic time it takes for the flow to become quasi-steady, the one-dimensional momentum equation leads to a non-dimensional relationship between the similarity parameter and the penetration depth that agrees well with most measurements. Departures from that prescription can be attributed to gravitational effects that are not accounted for in the one-dimensional theory.

I. INTRODUCTION

There is presently a strong interest in developing microthrusters for spacecraft propulsion. Two different types of applications are driving this interest. The first, primary propulsion for microspacecraft[1], requires thruster size and power consumption be reduced as the spacecraft size and available power shrink. The second, fine-positioning of spacecraft constellations for missions such as sparse-aperture interferometry[2], may require thrusters with micronewton and sub-micronewton thrust resolution.

Apart from the challenges associated with the design of microthrusters[3] are issues concerning propellant storage and handling. Propellant storage typically requires the carrying of additional tankage mass. Also, micro-valves currently under development for flow control have high leak rates[4]. We have addressed the issues associated with propellant handling in a previous paper[5] proposing that low vapor pressure liquid propellants could be passively controlled using capillary action. A system of this type is attractive because it is valveless and requires no additional tankage mass, other than the capillaries themselves.

A similarity parameter was defined in Ref. [5] based upon the collapse of data obtained in penetration experiments using a stepped capillary tube. However, the form of that similarity parameter was only applicable to the stepped-tube geometry. In the present work, which is a more fundamental study, we present a similarity parameter written in a form that can be applied to *any* one-dimensional capillary-driven flow. This parameter, which may be used for the optimization of microthruster mass flow rates, is of general importance to the fundamental understanding of capillary-driven flows.

A. Historical Perspective

The first analytical studies of surface tension and capillarity by Young[6] and Laplace[7] stated that at a liquid/vapor interface the difference between the liquid's pressure, p_l, and the vapor's pressure, p_v, is proportional to the total curvature of the interface itself. For a spherical meniscus, this can be written as

$$p_v - p_l = \frac{2\gamma}{R}\cos\theta, \tag{1}$$

where γ is the surface tension, θ is the contact angle, and R is the radius of the interface.

Hagen[8] and Poiseuille[9] later studied the flow of viscous liquids in circular pipes (including capillary tubes) and derived an equation for the steady-state volume flow rate based on the radial velocity profile for fully-developed flow given by

$$u(r) = \frac{1}{4\mu}\frac{\Delta p}{\Delta x}\left(a^2 - r^2\right), \tag{2}$$

where Δp is the total pressure drop in a column of fluid of length Δx, μ is the viscosity, and a is the tube radius. Reynolds experimentally tested the stability of this profile, finding that it held for laminar flows[10].

At the beginning of the 20^{th} century, there were several works concerned with the dynamics of fluid penetration into capillary tubes[11–15]. One of the results of these studies was the derivation of the Washburn equation[14] for

*Graduate Research Assistant. National Defense Science and Engineering Graduate Fellow.
†Chief Scientist at EPPDyL. Associate Professor, Applied Physics Group.
‡Presented at the 28^{th} International Electric Propulsion Conference, Toulouse, France.

laminar fluid penetration into a horizontal capillary. In the derivation it is assumed that the pressures at the tube inlet ($x = 0$) and in the air beyond the meniscus are equal. The pressure drop, Δp, over the length of the tube is time-independent and is given by Eq. (1) for a circular tube. If the flow is fully-developed and quasi-steady, then the velocity profile is given by Eq. (2) where Δx is replaced by the variable meniscus position x_* representing the distance the fluid penetrates into the tube in time t. Averaging over the velocity profile and integrating in time yields

$$x_*^2 = \frac{\Delta p\, a^2}{4\mu} t. \tag{3}$$

Recently, there have been many experimental and theoretical studies on the spreading rates of liquids flowing horizontally and in straight lines under capillary action. For example, liquids have been studied flowing in thin tubes[16], in surface grooves[17–21] and on microstrips[22]. All of these systems have been observed to follow Washburn-type dynamics, meaning the flow dynamics are functionally similar to Eq. (3) (i.e. $x_*^2 \propto t$).

B. Motivation & Organization

While the study of systems adhering to Washburn-type dynamics is a well developed field, no attempt has yet been made to find non-dimensional similarity parameters which would describe these flows. Consequently, capillary spreading data in the literature are typically presented in various dimensional forms, and the values of the relevant variables can be quite disparate depending on the geometry or fluid tested.

In this paper, we present a non-dimensional similarity parameter which is a combination of the relevant dimensional parameters of this problem. The similarity parameter is equivalent to the ratio of the average fluid velocity and a characteristic velocity, which is shown to be the maximum velocity for a quasi-steady capillary flow. Using the similarity parameter to non-dimensionalize published capillary spreading-rate data, a large set spanning five orders of magnitude in the fluid velocity, fourteen different fluids, and four different geometries can be collapsed into a single curve. To further collapse the data set of Ref. [5], we develop a phenomenological correction to account for gravitational effects, which are not included in the one-dimensional theory.

The data collapse implies that a universal relation for capillary flows exists. It is shown that the one-dimensional momentum equation recast in terms of the non-dimensional parameter leads to such a universal relation when the time scales are much longer than the characteristic time it takes for the flow to become quasi-steady.

The outline of the rest of this paper is as follows. In section II we introduce the similarity parameter that forms the basis of the paper. In section III we introduce the different experimental geometries to which the similarity parameter will be applied. Recent and previously published experimental data from these geometries are then presented and reduced to non-dimensional form in section IV as a means of evaluating the physical importance of the similarity parameter. In section V we address the condition under which the flow can be considered quasi-steady and provide a physical interpretation of the similarity parameter. Finally, in section VI, we discuss a universal scaling relation for these flows.

II. SIMILARITY PARAMETER

For this problem, the relevant dimensional parameters and their units are

$$[\langle u \rangle] = LT^{-1}, \quad [a] = L, \quad [x_*] = L,$$
$$[\mu] = ML^{-1}T^{-1}, \quad [\Delta p] = ML^{-1}T^{-2},$$

where $\langle u \rangle$ is the average fluid velocity and a is a characteristic length (the radius for capillary tubes). The surface tension, while not explicitly in this list, is implicitly included because the total pressure drop in these systems is a function of the surface tension as well as the geometry of the problem.

The Buckingham Pi theorem states that we should be able to find two independent, dimensionless parameters by combining the above dimensional parameters. Two such independent parameters are the similarity parameter,

$$\Pi = \frac{\langle u \rangle\ \mu}{a\, \Delta p}, \tag{4}$$

and the non-dimensional length,

$$X = \frac{x_*}{a}. \tag{5}$$

We see that, physically, Π is the ratio of the competing effects of viscosity and the driving pressure, which is a function of the surface tension. We also recognize that Π is similar to the well known Capillary number, $\mathrm{Ca} = \langle u \rangle\, \mu/\gamma$. However, by including the total pressure drop in our list of dimensional parameters instead of the surface tension, we can tailor the final form of Π to different geometric configurations.

Note that Π is also equivalent to a ratio of two velocities. Based on this, we can define a characteristic velocity for capillary flows

$$U_{cap} = \frac{a\, \Delta p}{\mu}, \tag{6}$$

and rewrite Π as

$$\Pi = \frac{\langle u \rangle}{U_{cap}}. \tag{7}$$

We shall defer to section V an explanation of the physical meaning of U_{cap}.

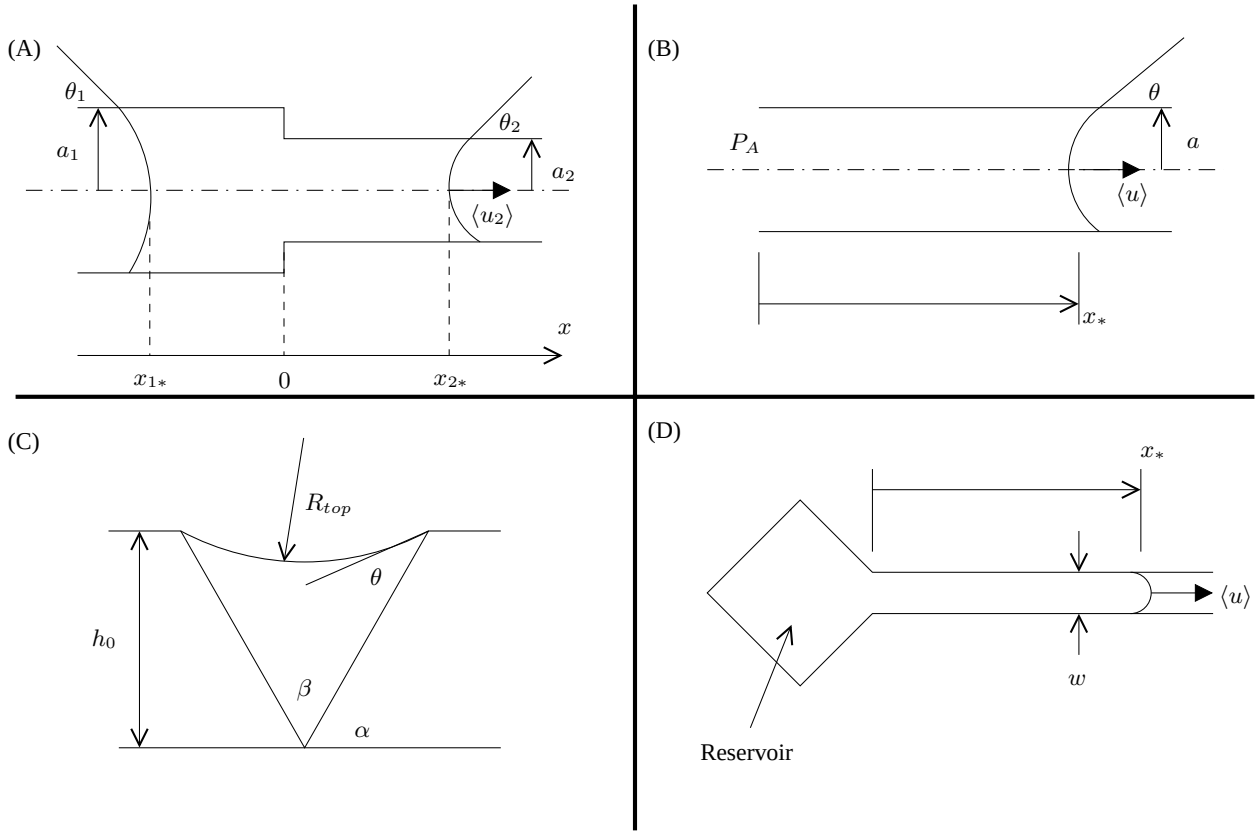

FIG. 1: (A) A schematic of the stepped capillary tube geometry. (B) Schematic of a single tube geometry. (C) A view looking along the channel of the V-groove geometry (after Ref. [19]). (D) A view looking down on the microstrip geometry (after Ref. [22]).

Had time been added to the list of relevant dimensional parameters, an additional non-dimensional parameter, such as $t\Delta p/\mu$, would need to be added to our list of dimensionless variables. However, as we show in section IV, the collapse of the data is attained without invoking time. We also show, in section V, that the irrelevance of time is due to the quasi-steady condition prevailing in all the considered flows.

III. EXPERIMENTAL GEOMETRIES

In this paper, we apply the derived similarity parameters to data sets from four different geometries (see Fig. 1). The geometries analyzed are: (A) a stepped capillary tube, (B) a single capillary tube, (C) a V-shaped groove, and (D) a hydrophilic microstrip. In the following text, we describe each geometry and the experiments that were originally performed and attempt to write Π and X in terms of relevant, measurable variables. We shall find that the variable that is most difficult to determine in all these cases is the total pressure drop, Δp, over the length of the capillary

A. Stepped Tube

We conducted experiments using the geometry shown in Fig. 1A and first reported the results in Ref. [5]. All quantities with a subscript of 1 denote values in the larger radius tube while the subscript 2 denotes values in the smaller radius tube. Initially, fluid was injected into the larger radius tube until the meniscus reached the smaller radius tube. Once the fluid entered the smaller radius tube, all active injection was halted.

Five different capillary tube radius combinations were tested. In addition to varying the radii, five different fluids were tested, where the fluid properties are given in Table I. The properties for methanol and propanol-2 were taken from Ref. [23]. The viscosities of the other three fluids were taken from manufacturer data (Ref. [24] for dibutyl phthalate and Ref. [25] for the mechanical and diffusion pump oils). The listed surface tensions for these three fluids were found by measuring the capillary rise in several different radius tubes. The contact angles were found by visually measuring the radius of the meniscus and comparing that with the tube radius. The ratio of these two radii was set equal to $\cos\theta$.

To write out the non-dimensional parameters, we must first find a solution for the average fluid velocity, $\langle u_2 \rangle$. Tak-

TABLE I: Stepped capillary tube fluids and their properties. Data with error bars were measured by the authors.

Name	γ[mN/m]	μ[mPa-s]	θ[deg]
methanol (CH_4O)	22.1	0.54	0
propanol-2 (C_3H_8O)	20.9	2.04	0
dibutyl phthalate ($C_{16}H_{22}O_4$)	33.9 ($\pm$3.3)	20.3	62.3 ($\pm$3.2)
Fisherbrand 19 mechanical pump oil	30.5 ($\pm$3.6)	47.9	63.0 ($\pm$6.1)
Invoil 940 Si-diffusion pump oil	34.0 ($\pm$4.4)	25.9	63.9 ($\pm$4.7)

ing the pressure gradient, dP/dx, equal to a constant k in each tube, we can average Eq. (2) over the cross-sectional area of the flow to obtain an average velocity

$$\langle u_2 \rangle = \frac{k_2 a_2^2}{8\mu}. \tag{8}$$

The incompressible continuity equation ($\langle u \rangle A$ = a constant) results in the compatibility condition

$$k_1 = \left(\frac{a_2}{a_1}\right)^4 k_2. \tag{9}$$

We bring closure to this formulation by assuming a pressure profile in the fluid (see Fig. 2). The meniscus at each end is exposed to the same outside pressure, and it is known from Eq. (1) that the discontinuities in the pressure at each meniscus will be

$$\Delta P_1 = \frac{2\gamma}{a_1}\cos\theta_1, \tag{10a}$$

$$\Delta P_2 = \frac{2\gamma}{a_2}\cos\theta_2. \tag{10b}$$

Using Eqs. (9) and (10) and the fact that the pressure is piecewise continuous between the menisci (see Fig. 2), analytical expressions for k_1 and k_2 can be found[27]. These are

$$k_1 = \frac{2\gamma\left(\cos\theta_2/a_2 - \cos\theta_1/a_1\right)}{x_{2*} - x_{1*}\left(a_2/a_1\right)^4}\left(a_2/a_1\right)^4, \tag{11a}$$

$$k_2 = \frac{2\gamma\left(\cos\theta_2/a_2 - \cos\theta_1/a_1\right)}{x_{2*} - x_{1*}\left(a_2/a_1\right)^4}. \tag{11b}$$

Note from the coordinate system that x_{1*} is measured such that it is always negative, so the denominators in these expressions are always positive.

It is worth noting that the quantity x_{eq*}, which we define as

$$x_{eq*} \equiv x_{2*} - x_{1*}\left(a_2/a_1\right)^4 \tag{12}$$

has a physical interpretation. It is the length of a column of fluid of radius a_2 and constant pressure gradient k_2 having a pressure drop equal to the total pressure drop between the two menisci. In other words, $|k_2 x_{eq*}| = |k_1 x_{1*}| + |k_2 x_{2*}|$.

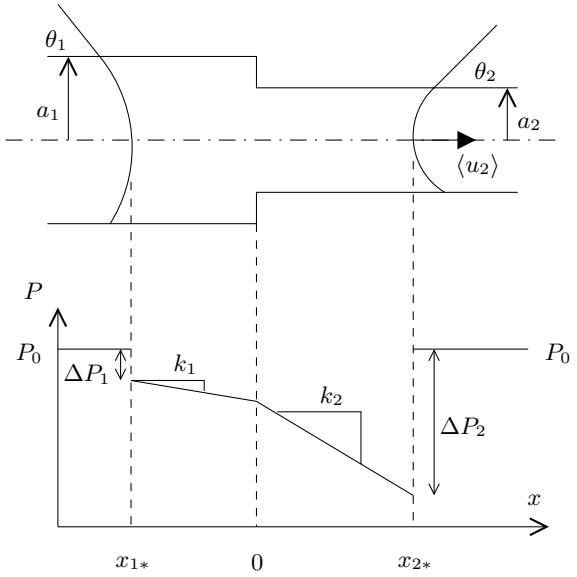

FIG. 2: Pressure profile in a stepped capillary tube.

We can now write k_2 as $\Delta p/x_{eq*}$ and express the similarity parameter, Eq. (4), as

$$\Pi = \frac{\langle u_2 \rangle \mu}{2\gamma}\frac{1}{a_2\left(\cos\theta_2/a_2 - \cos\theta_1/a_1\right)}, \tag{13}$$

and the dimensionless length, Eq. (5), as

$$X = \frac{x_{eq*}}{a_2}, \tag{14}$$

where the radius, a_2, is used as the characteristic length.

B. Single Tube

Fisher and Lark[16] collected data for fluids flowing in thin capillaries. They measured the value of x_*^2/t for different tube radii (see Fig. 1B). These experiments were conducted using both water (γ/μ = 72.7 m/s, $\theta = 0^\circ$) and

cyclohexane ($\gamma/\mu = 22.1$ m/s, $\theta = 8°$) as the working fluid. The goal in that work was to verify the applicability of the Washburn equation, Eq. (3), for very small tube radii[28].

We see that a single tube is a special case of a stepped capillary tube where $a_1 \to \infty$. Using this fact allows us to simplify the similarity parameter and non-dimensional length given in Eqs. (13) and (14) to

$$\Pi = \frac{\langle u \rangle \mu}{2\gamma} \frac{1}{\cos\theta}, \tag{15a}$$

$$X = \frac{x_*}{a}. \tag{15b}$$

Note that this form assumes the pressure at the immersed end of the tube is equal to the vapor pressure at the fluid/vapor interface (typically the atmospheric pressure, P_0). However, as long as the flow can be considered quasi-steady, Eq. (15a) can be generalized to account for an arbitrary pressure, P_A, at the immersed end. In that case, the pressure difference over the length of the fluid is

$$\Delta p = P_A - \left[P_0 - \left(2\gamma\cos\theta\right)/a\right],$$

and Π takes on the more general form

$$\Pi = \frac{\langle u \rangle \mu}{2\gamma} \frac{1}{\left(\left[\left(P_A - P_0\right)a\right]/\left(2\gamma\right) + \cos\theta\right)}. \tag{16}$$

C. V-shaped Grooves

For fluids flowing in V-shaped grooves, we use data found in Ref. [19]. The geometry that was employed in these experiments (see Fig. 1C) consisted of a groove of angle β and height h_0 being fed from a liquid reservoir. Multiple groove angles, groove heights, and liquids were tested, with each test's properties listed in Table II.

A solution for the pressure drop over the length of the groove can be determined from Ref. [19]. In that work, the authors found that the governing equation for the spreading could be written as

$$x_*^2 = K\left(\theta, \alpha\right) \frac{\gamma h_0}{\mu} t, \tag{17}$$

where the angle α is shown in Fig. 1C. If we assume that the flow is fully-developed and quasi-steady, it will have a form similar to that of the Hagen-Poiseuille flow of Eq. (2). Averaging Eq. (2) over the velocity profile and recasting it in terms of our dimensional variable list yields

$$\langle u \rangle = \frac{\Delta p}{x_*} \frac{a^2}{8\mu}, \tag{18}$$

where a is the characteristic length. Integrating the average velocity with respect to time yields the Washburn equation [Eq. (3)]. Setting $a = h_0$ and comparing Eqs. (17) and (3), it is evident that the pressure drop is given by the expression

$$\Delta p = \frac{4\gamma K\left(\theta, \alpha\right)}{h_0}. \tag{19}$$

TABLE II: Fluids tested in V-shaped grooves and their properties (from Ref. [19]).

	γ/μ	$K\left(\theta,\alpha\right)^{1/2}$	
liquid	[cm/s]	exptl	Eq. (20)
1,4-butanediol	59.5	0.245	0.282
cyclohexanol	58.2	0.247	0.301
1-butanol	941	0.270	0.301
2-octanol	408	0.259	0.297
diethylene glycol	162	0.231	0.273
1-heptanol	489	0.249	0.297
1,4-butanediol	59.5	0.244	0.219
cyclohexanol	58.2	0.275	0.248
1-butanol	941	0.294	0.248
2-octanol	408	0.298	0.241
diethylene glycol	162	0.187	0.204
1-heptanol	489	0.281	0.241
cyclohexanol	58.2	0.190	0.174
1-butanol	941	0.194	0.174
2-octanol	408	0.202	0.166
1-heptanol	489	0.199	0.166

Several analytical solutions for K have been found[18, 19], each involving a different assumption regarding the radius of curvature of the top surface of the fluid, R_{top} (see Fig. 1C). The solution for K that is generally closest to the experimentally determined value is based on a flat topped fluid ($R_{top} = \infty$) and is given by

$$K\left(\theta, \alpha\right) = \frac{1}{2\pi\sin\left(\alpha\right)} \left[\cos\left(\theta\right) - \frac{\left(\alpha - \theta\right)\cos\left(\alpha\right)}{\sin\left(\alpha - \theta\right)}\right], \tag{20}$$

where the angle α is shown in Fig. 1C. This allows us to write the similarity parameter and dimensionless length for this geometry as

$$\Pi = \frac{\langle u \rangle \mu}{4\gamma} \frac{1}{K\left(\theta, \alpha\right)}, \tag{21a}$$

$$X = \frac{x_*}{h_0}. \tag{21b}$$

D. Microstrips

Darhuber *et al.*[22] conducted experiments using hydrophilic microstrips etched onto a hydrophobic background (see Fig. 1D). The microstrips were connected to a reservoir pad of the same hydrophilic material. A quantity of the working fluid (polydimethylsiloxane silicone oil [Fluka], $\gamma/\mu = 1.03$ m/s) was deposited on the reservoir pad and the fluid then spread along the microstrip through capillary action. In that study it was found that the spreading was governed by Eq. (17).

Using the methods of Ref. [18], Darhuber *et al.*[22] determined for this geometry the variation of K with the strip width. Unlike the V-shaped grooves, there are no known fully-analytical solutions for K in this geometry. However,

it was found that the average streamwise velocity should vary according to the relation

$$\langle u \rangle = \frac{K}{2x_*}\frac{\gamma a}{\mu} \propto \frac{\gamma w^4}{\mu}\frac{1}{x_*}, \tag{22}$$

where w is the strip width, which we shall take as the characteristic length scale. To determine Δp for this case, we compare Eq. (22) with Eq. (18) and obtain

$$\Delta p = \frac{8\gamma w^2}{\zeta}, \tag{23}$$

where we have multiplied the far right hand side of Eq. (22) by the proportionality constant ζ^{-1}. We can now write the similarity parameter and dimensionless length as

$$\Pi = \frac{\langle u \rangle \mu}{8\gamma}\frac{\zeta}{w^3}, \tag{24a}$$

$$X = \frac{x_*}{w}. \tag{24b}$$

Note that ζ is a factor with dimensions of length-cubed. If Eq. (23) accurately tells how Δp varies with w and γ, then ζ should be a constant for a given fluid irrespective of the strip width or surface tension.

IV. EXPERIMENTAL DATA

In this section, we shall present experimental data for each of the four geometries previously discussed. These data will first be plotted in dimensional coordinates and then replotted using their respective non-dimensional prescriptions. We shall show that, for all cases, the non-dimensional parameter collapses these data, i.e. significantly reduces the range of data spread in one of the variables. The stepped capillary tube data set and discussion will be deferred to the end of this section as we will be required to develop and apply a correction which need not be applied to the other data sets.

A. Single Tube

Fisher and Lark[16] presented data for the penetration rates of fluids into very fine capillaries. These data were originally presented in coordinates of penetration depth squared per unit time and capillary radius. If a Hagen-Poiseuille flow having a constant pressure drop is assumed, Eq. (3) allows us to state that the value of x_*^2/t should be a constant, $\mathcal{G}$, for a single fluid and radius. To obtain velocities from these data, we simply differentiate $x_*^2 = \mathcal{G}t$ to obtain $\langle u \rangle = \mathcal{G}/2x_*$. For comparing the various data sets, we took $x_* = 50$ mm for all single tube data. The data, non-dimensionalized using Eqs. (15), are replotted in Fig. 3B.

We see that the data for both water and cyclohexane do collapse to a single curve. The deviation from this curve at larger values of X is due to the larger relative error in determining the values of x_*^2/t at smaller values of a.

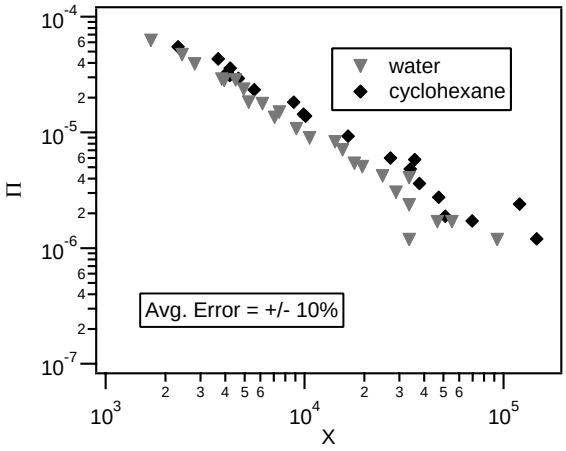

FIG. 3: Data from Fisher and Lark[16] for fluid penetration rates into a single tube expressed using the non-dimensionalization given in Eqs. (15).

B. V-shaped Grooves

Data sets for fluids flowing into V-shaped grooves are taken from Ref. [19]. The fluids tested and their properties are listed in Table II. Included in this table are the values of $K(\theta,\alpha)^{1/2}$ that were computed in Ref. [19], where column 3 is the experimentally determined value and column 4 is the value computed using Eq. (20). The non-dimensional data set for $\beta = 45^\circ$ is found in Fig. 4(A-B), for $\beta = 77^\circ$ is found in Fig. 4(C-D), and for $\beta = 124^\circ$ is found in Fig. 4(E-F). The velocities were determined in a manner nearly identical to that used for the single tube geometry.

We see from the plots in Fig. 4 that not only can the data all be collapsed to one curve for each angle β (as Rye *et al.*[19] showed), but also that the similarity parameter collapses the data from all groove-angles tested to the same curve. Finally, we see that the analytical expression for $K(\theta,\alpha)$ [Figs. 4(A, C & E)] yields values of Π that are very close to those computed using the experimentally determined values of $K(\theta,\alpha)$ [Figs. 4(B, D & F)] in all cases, leading us to conclude that Eq. (20) is a good expression for $K(\theta,\alpha)$.

C. Microstrips

Experimental data for polydimethylsiloxane silicone oil [Fluka] spreading on hydrophilic microstrips[22] are presented in non-dimensional form [Eqs. (24)] in Fig. 5. The proportionality constant ζ has been treated as a free parameter in this case. Its value has been chosen such that the data agree with the universal scaling relation presented in section VI. The value of ζ used to non-dimensionalize these data was 5.55×10^{-6} m^3 or $\zeta^{1/3} = 1.77$ cm.

As shown in Fig. 5(B), all four data sets effectively collapse onto a single curve when this value of ζ is used to

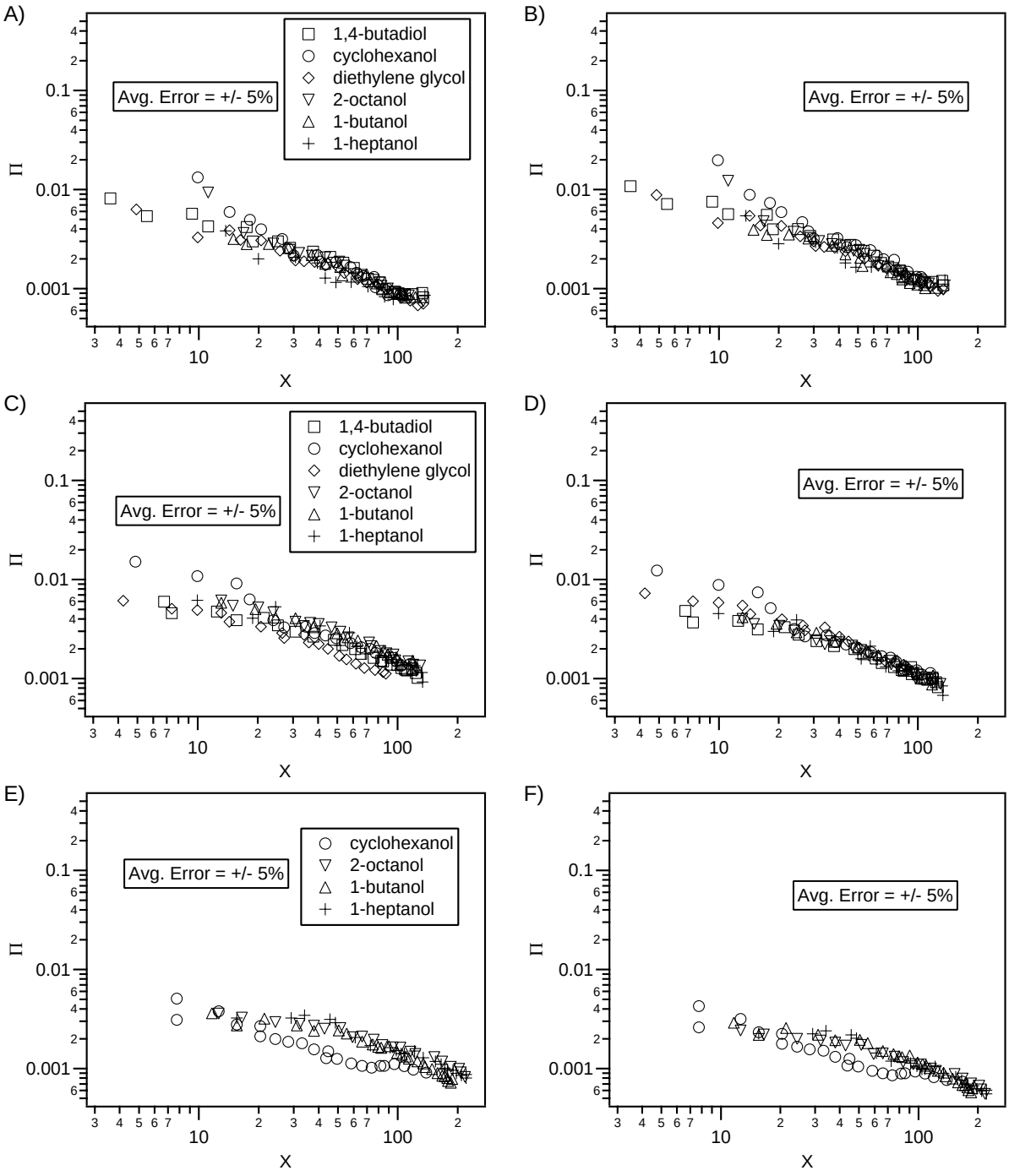

FIG. 4: Penetration data from Ref. [19] for fluids flowing in V-shaped grooves cut with an angle $\beta = 45^{\circ}$ (A & B), 77° (C & D) and 124° (E & F) plotted using the non-dimensional prescription given in Eqs. (21) with the value of $K\left(\theta,\alpha\right)$ (A, C & E) given by Eq. (20) and (B, D & F) computed by Rye *et al.*[19] from a curve fit of the experimental data.

compute Π. However, the *collapse* is independent of the numerical choice of ζ, as long as it is a constant. This further validates the relevance of the non-dimensionalization prescribed by Eqs. (24).

D. Stepped Tube

Experimental data for fluids flowing in stepped capillary tubes (see Ref. [5]) are shown in Fig. 6. These data are divided into two groups, each corresponding to a given radius, a_1 (see Fig. 1A). In Figs. 6(A & B), the data have

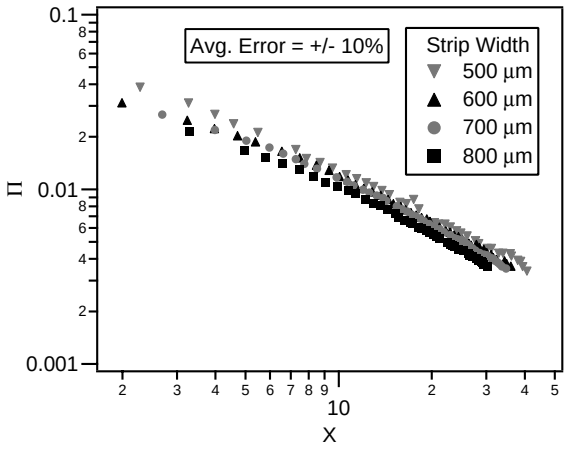

FIG. 5: Penetration data from Ref. [22] for polydimethylsiloxane silicone oil flowing on microstrips of varying widths, w, plotted using the non-dimensionalization given by Eqs. (24) where ζ has been taken equal to 5.55×10^{-6} m^3 for all widths.

been non-dimensionalized according to Eqs. (13) and (14). We notice that, while non-dimensionalizing does collapse the data significantly, the spread is still a little more than an order of magnitude.

Gravitational Correction

At this point, it is convenient for us to introduce the Bond number, which is defined as the ratio of gravitational to surface tension forces and is written as

$$\text{Bo} = \frac{\rho g d^2}{\gamma}, \tag{25}$$

where ρ is the fluid density and d is the capillary tube diameter. The data set in Fig. 6 has Bo $\sim \mathcal{O}(0.1-1)$, implying that gravitational forces and their associated two-dimensional effects, neglected in the theoretical treatment of this problem, may be important. In fact, we expect these neglected effects to cause the non-dimensionalization to begin to fail for values of Bo $\geq \mathcal{O}(0.1)$. However, inspired by experimental observations, we have developed an empirical model which, for the values of Bo spanned by these experiments, corrects for the effects of gravity.

It is experimentally observed that the meniscus deforms with increasing Bo. This deformation increases the meniscus radius, R_m, as shown schematically in Fig. 7. We sought a simple, first-order scaling relation to effectively account for this increase in radius and yield a small correction to the formula for Π given in Eq. (13).

It is convenient to define a reference condition where the gravitational effects are small. We define our reference as the case where Bo $= 0.1$. We now define an effective meniscus radius, R_{eff}, that can be used to modify Eq. (13). The quantity R_{eff}/R, where R is the tube's physical radius, is expected to be more a function of Bo than of Π and X. We attempt to correct the gravitationally-induced departure in the data using the following proposed phenomenological scaling which is not derived from first principles. Since the Bond number is a function of the radius squared, we propose that the effective radius increases monotonically with Bo$^{1/2}$ and goes to the tube radius (for a fully wetting fluid) as Bo goes to zero. Denoting the reference condition as Bo$_*$, we write this proposed scaling as[29]

$$R_{eff} = R\left(1 + \sqrt{\frac{\text{Bo}}{\text{Bo}_*}}\right). \tag{26}$$

Applying this scaling to the radius terms inside the parentheses in Eq. (13), we obtain the modified expression

$$\Pi = \frac{\langle u_2 \rangle \mu}{a_2} \frac{1}{\Delta p'}, \tag{27}$$

where $\Delta p'$ is the modified pressure drop:

$$\Delta p' = \frac{2\gamma\cos\theta_2}{a_2\left(1+\sqrt{\text{Bo}_2/\text{Bo}_*}\right)} - \frac{2\gamma\cos\theta_1}{a_1\left(1+\sqrt{\text{Bo}_1/\text{Bo}_*}\right)}.$$

The values of the Bond number evaluated at the leading and trailing menisci are Bo$_2$ and Bo$_1$ respectively.

The data found in Figs. 6(C & D) are plotted using the modified Π given in Eq. (27) with the values of Bo$_{1,2}$ given

TABLE III: Bond numbers, Bo$_2$, for all experiments using stepped capillary tubes.

fluid	radius (a) [mm]	Bo
methanol	0.30	0.126
	0.60	0.506
	1.35	2.55
	1.50	3.15
propanol-2	0.30	0.141
	0.60	0.564
	1.10	1.89
	1.35	2.86
	1.50	3.53
dibutyl phthalate	0.30	0.230
	0.60	0.922
	1.10	3.10
	1.35	4.66
	1.50	5.75
mechanical pump oil	0.30	0.219
	0.60	0.878
	1.10	2.95
	1.35	4.43
	1.50	5.48
diffusion pump oil	0.30	0.236
	0.60	0.945
	1.10	3.18
	1.35	4.78
	1.50	5.90

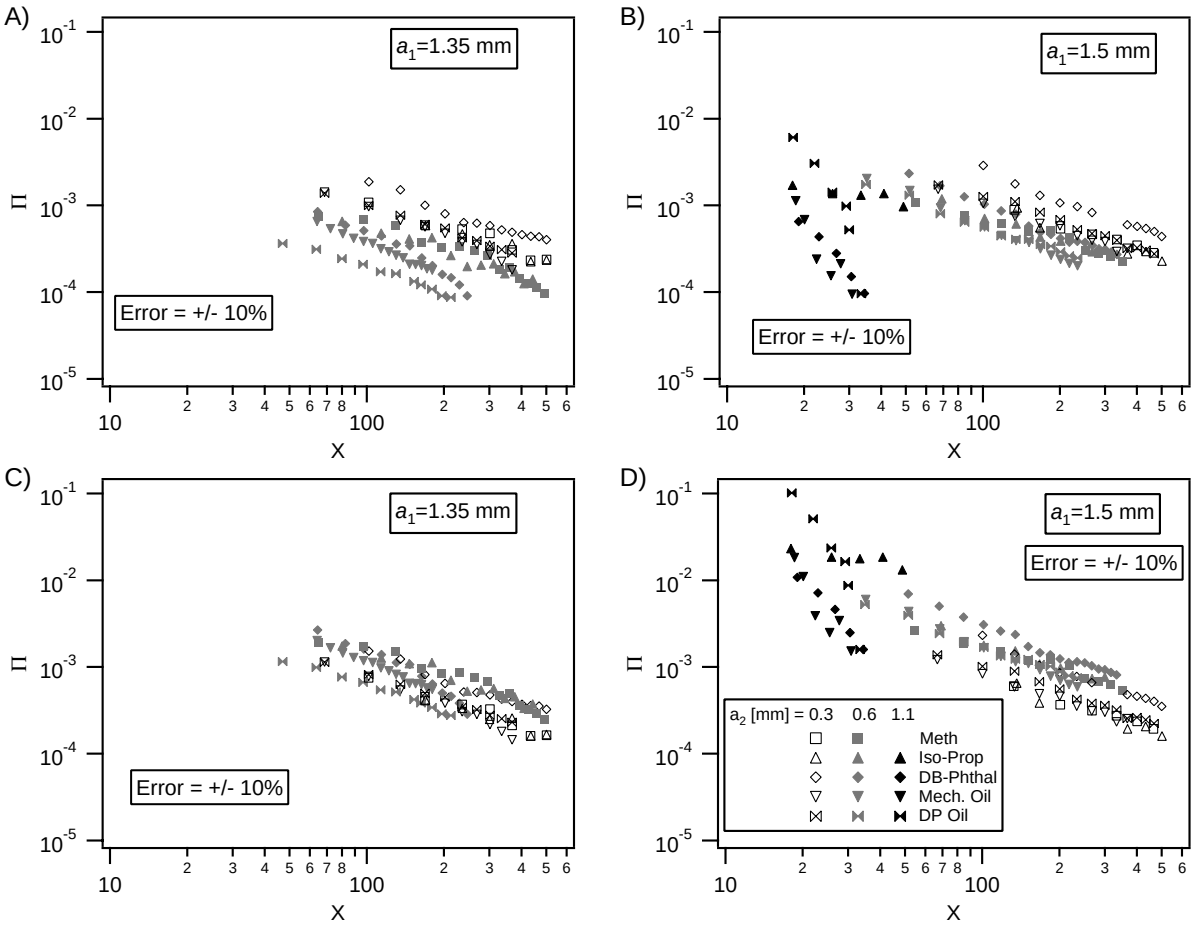

FIG. 6: (A)-(B) Penetration data from Ref. [5] for fluids flowing in stepped capillary tubes plotted using the non-dimensionalization of Eqs. (13) and (14) (a_1 as noted on the graphs). (C)-(D) The non-dimensional data replotted using the gravitational correction given in Eqs. (27). Note that the legend for all plots is also shown in (D).

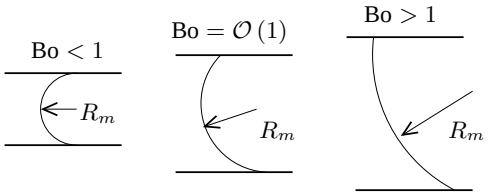

FIG. 7: Schematic showing how the meniscus deforms with increasing Bo.

in Table III. We see that the proposed gravitational correction further collapses these data by up to a factor of five, showing that this phenomenological correction, to first order, represents the effect of gravity.

V. THE QUASI-STEADY REGIME

In the appendix, we show that the momentum equation for a flow entering a capillary tube from a semi-infinite reservoir can be written as

$$\frac{B\tau^2}{a^2}\left[\left(x_* + \frac{a}{2}\right)\frac{d^2x_*}{dt^2} + \frac{1}{8}\left(\frac{dx_*}{dt}\right)^2\right] = 1 - \frac{x_*\tau}{a^2}\frac{dx_*}{dt}. \tag{28}$$

In this equation, τ and B are, respectively, a dimensional timescale and a dimensionless parameter and are defined

$$\tau = \frac{8\mu}{\Delta p}, \quad B = \frac{\rho a^2}{\tau^2 \Delta p} = \frac{\rho a^2 \Delta p}{(8\mu)^2}.$$

Also, x_*, dx_*/dt, and d^2x_*/dt^2 are, respectively, the position, velocity and acceleration of the moving air-liquid interface.

A. Dimensionless Formulation and Solution

Introducing the dimensionless variables X and ξ,

$$X = \frac{x_*}{a}, \quad \xi = \frac{t}{\tau} = \frac{t\Delta p}{8\mu},$$

we can rewrite Eq. (28) as

$$B\left[\left(X + \frac{1}{2}\right)\frac{d^2X}{d\xi^2} + \frac{1}{8}\left(\frac{dX}{d\xi}\right)^2\right] = 1 - X\frac{dX}{d\xi}. \quad (29)$$

For problems of interest, the condition $X \geq 1$ should be satisfied. We notice that if the left hand side of Eq. (29) is negligible, the solution is

$$X = \sqrt{2\xi}, \quad (30)$$

which is the non-dimensional version of the Washburn equation [Eq. (3)].

Consistent with the Washburn solution we have

$$\left(\frac{dX}{d\xi}\right)^2 = \frac{1}{2\xi}, \quad X\frac{d^2X}{d\xi^2} = -\frac{1}{2\xi}. \quad (31)$$

In order for the left hand side of Eq. (29) to be negligible, the inequality $B << \xi$ must be satisfied. Rewriting this inequality in terms of dimensional parameters, we obtain

$$t_{CO} \equiv \frac{\rho a^2}{8\mu} << t, \quad (32)$$

where t_{CO} is the "crossover" time. This implies that for the flow to be considered quasi-steady, the time must be much greater than t_{CO}, which is essentially the time it takes for viscous diffusion to travel a distance $\mathcal{O}(a)$.

B. Meaning of U_{cap}

If we operate at a time that satisfies the inequality in Eq. (32), we can substitute for time using the first of Eqs. (31). Substituting and rearranging yields the expression

$$2\frac{\rho\, U_{cap}\, a}{\mu}\left(\frac{\langle u\rangle}{U_{cap}}\right)^2 = 2\,\mathrm{Re}|_{U_{cap}}\,\Pi^2 << 1, \quad (33)$$

where $\mathrm{Re}|_{U_{cap}}$ is a Reynold's number based on the characteristic velocity U_{cap}. For most practical flows such as those discussed here $\mathrm{Re}|_{U_{cap}} \geq \mathcal{O}(1)$.

We know that as $\langle u\rangle \rightarrow U_{cap}$, $\Pi \rightarrow 1$. When this occurs the inequality in Eq. (33) is violated and the flow cannot be considered quasi-steady. We conclude that U_{cap} is a characteristic velocity for capillary flows. For times later than t_{CO}, the flow becomes quasi-steady, the inequality in Eq. (33) holds, and the fluid velocity is always less than U_{cap} [30]. Since $\langle u\rangle$ is less than U_{cap} for all the developed flows considered in this paper, we conclude that these flows are essentially quasi-steady.

VI. SCALING RELATION

In this section, we turn our attention to the problem of finding a relationship between the similarity parameter, Π, and the non-dimensional length, X. For times greater than t_{CO}, we can set the left hand side of Eq. (29) equal to zero and then rearrange the right hand side to obtain

$$\frac{dX}{d\xi} = X^{-1} \quad (34)$$

Writing the left hand side of this equation in terms of the similarity parameter yields the universal relation

$$\Pi = \frac{1}{8}X^{-1}. \quad (35)$$

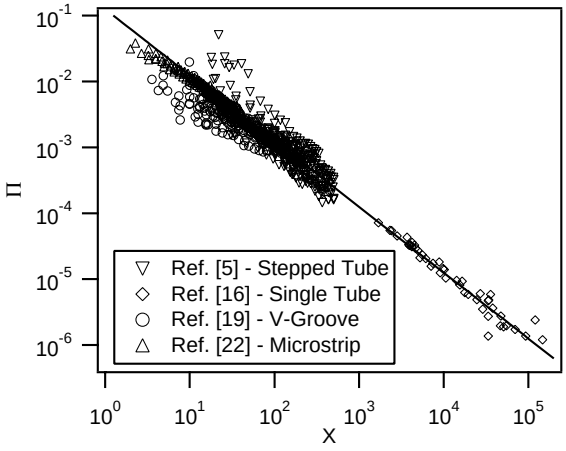

FIG. 8: All penetration data contained within this paper plotted in coordinates of Π and X. In addition, Eq. (35), representing the universal scaling relation, is plotted.

In Fig. 8, we have plotted all the data presented in this paper using the variables Π and X. In addition, the line given by Eq. (35), representing the scaling relation between the non-dimensional parameters, has been plotted. This plot shows that, not only do all the data, independent of geometry or fluid, effectively collapse[31] to a single curve, but that this curve is given by the scaling relation.

VII. CONCLUSIONS

This study leads to the following major conclusions.

- A similarity parameter for quasi-steady fluids advancing into horizontal capillaries exists and can be found by combining the relevant dimensional parameters of this problem.
- The similarity parameter consists of the ratio between either the effect of viscosity and that of the driving pressure, or the average fluid velocity and

a characteristic capillary velocity, U_{cap}. When the time is greater than the "crossover" time, the characteristic velocity is greater than the fluid velocity.

- The similarity parameter collapses a large data set spanning five orders of magnitude in penetration velocity, fourteen different fluids, and four different geometries to a single line. This implies that a relation between the similarity parameter, $\Pi = \langle u \rangle / U_{cap}$, and the non-dimensional distance, X, exists.

- The equation $\Pi = (1/8)\, X^{-1}$, which holds for fully-developed quasi-steady flows (i.e. for times much greater than $\rho a^2/8\mu$), provides a universal scaling relation that agrees well with the collapsed data set over a large range of experimental parameters.

- The scaling begins to fail as Bo approaches unity due to gravitational effects, which are not accounted for in the one-dimensional model. However, these effects can, to first order, be accounted for by applying a phenomenological correction to Π.

Acknowledgments

This work has greatly benefited from the insightful comments of Prof. S.H. Lam.

We also acknowledge several discussions with Dr. A.A. Darhuber and Dr. P.G. Felton.

APPENDIX: ORIGIN OF EQ. (28)

1. Formulation

Consider a straight, round, semi-infinite tube of radius a. This tube extends in the positive x-direction and it is connected to a much larger radius tube in the negative x-direction. At $t \leq 0$, liquid fills the $x \leq 0$ side and there is no liquid in the $x > 0$ portion of the tube. At $t > 0$, liquid is expected to enter the narrow tube. The static pressures at $x = \pm\infty$ are identical and denoted by p_0. The static pressure on the liquid side of the liquid-air interface is reduced by the surface tension and is given by Eq. (1). For the moment, we shall take the pressure reduction due to surface tension to be equal to Δp. Let x_* denote the location of the moving air-liquid interface and $\langle u \rangle$ denote its average velocity, or

$$\langle u \rangle = \frac{dx_*}{dt}, \quad 0 \leq x \leq x_*, \quad t \geq 0. \tag{A-1}$$

Note that we can rewrite the parabolic velocity profile, Eq. (2), as

$$u\left(r\right) = 2\left\langle u \right\rangle \left(1 - \frac{r^2}{a^2}\right). \tag{A-2}$$

2. Static Pressure at $x \approx 0$

The liquid at $x < 0$ converges and flows toward the entrance of the narrow tube. The static pressure at $x \approx 0$ is less than p_0. For the region where $x < 0$, we can use Bernoulli's equation for an inviscid, unsteady flow[32]

$$p_0 = p + \rho\left(\frac{V^2}{2} + \frac{\partial \phi}{\partial t}\right) = \text{constant}, \tag{A-3}$$

where ϕ is the velocity potential defined as

$$\mathbf{V} = \nabla \phi, \tag{A-4}$$

and $\mathbf{V}$ is the liquid velocity vector of magnitude V. Equating the flowrate into the narrow tube with the flowrate through any tube cross-section, we can find a simple sink velocity potential:

$$\phi = \frac{\langle u \rangle\, a^2}{2r}, \tag{A-5}$$

where r is the radial spherical coordinate. We can now evaluate Eq. (A-3) at $x \approx 0$ as

$$p\left(x \approx 0\right) = p_0 - \rho\left(\frac{1}{8}\left(\frac{dx_*}{dt}\right)^2 + \frac{a}{2}\frac{d^2x_*}{dt^2}\right), \tag{A-6}$$

where the dynamic pressure and unsteady term in Eq. (A-3) were evaluated at $r = a$. The time-dependent pressure gradient in the narrow tube is expected to be a constant with respect to x. This can be computed by

$$\begin{aligned}\frac{\partial p}{\partial x} &= \frac{\left(p_0 - \Delta p\right) - p\left(x \approx 0\right)}{x_*}, \\ &= -\frac{\Delta p}{x_*} + \frac{\rho}{x_*}\left(\frac{1}{8}\left(\frac{dx_*}{dt}\right)^2 + \frac{a}{2}\frac{d^2x_*}{dt^2}\right).\end{aligned} \tag{A-7}$$

3. x-Momentum Equation

The x-momentum equation in the narrow tube is

$$\rho\frac{\partial \left\langle u \right\rangle}{\partial t} = -\frac{\partial p}{\partial x} + \mu\nabla^2 u\left(r\right). \tag{A-8}$$

Taking $u\left(r\right)$ to be given by Eq. (A-2), we can rewrite the momentum equation as

$$\rho\frac{\partial \left\langle u \right\rangle}{\partial t} = -\frac{\partial p}{\partial x} - \frac{8\mu\left\langle u \right\rangle}{a^2}. \tag{A-9}$$

Substituting Eq. (A-7) for the pressure gradient and rearranging we obtain

$$\frac{B\tau^2}{a^2}\left[\left(x_* + \frac{a}{2}\right)\frac{d^2x_*}{dt^2} + \frac{1}{8}\left(\frac{dx_*}{dt}\right)^2\right] = 1 - \frac{x_*\tau}{a^2}\frac{dx_*}{dt}, \tag{A-10}$$

where we have defined a dimensional timescale, τ, and a dimensionless parameter, B, as

$$\tau = \frac{8\mu}{\Delta p}, \quad B = \frac{\rho a^2}{\tau^2 \Delta p} = \frac{\rho a^2 \Delta p}{(8\mu)^2}.$$

Equation (A-10) is exactly Eq. (28).

[1] J. Wong, H. Reed, and A.D. Ketsdever. "University micro-/nanosatellite as a micropropulsion testbed". In *Micropropulsion for Small Spacecraft*, Ch. 2, edited by M.M. Micci and A.D. Ketsdever, Vol. 187, Progress in Aeronautics and Astronautics, AIAA, Reston, VA, 2000, pp. 25-44.

[2] LISA Science Working Group. *LISA Mission Concept Study: Laser Interferometer Space Antenna for the Detection and Observation of Gravitational Waves*. edited by W.M. Folkner, P.L. Bender and R.T. Stebbins, NASA Jet Propulsion Lab., JPL Publ. 97-16, California Inst. of Technology, Pasadena, CA, 1997.

[3] J. Mueller. "Thruster options for microspacecraft: A review and evaluation of state-of-the-art and emerging technologies". In *Micropropulsion for Small Spacecraft*, Ch. 3, edited by M.M. Micci and A.D. Ketsdever, Vol. 187, Progress in Aeronautics and Astronautics, AIAA, Reston, VA, 2000, pp. 45-138.

[4] J. Mueller. "Review and applicability assessment of MEMS-based microvalve technologies for microspacecraft propulsion". In *Micropropulsion for Small Spacecraft*, Ch. 19, edited by M.M. Micci and A.D. Ketsdever, Vol. 187, Progress in Aeronautics and Astronautics, AIAA, Reston, VA, 2000, pp. 449-476.

[5] K.A. Polzin and E.Y. Choueiri, "A passive propellant feeding mechanism for micropropulsion using capillarity", In *38th AIAA/ASME/SAE/ASEE Joint Propulsion Conference*, Indianapolis, IN, 2002. AIAA Paper 2002-3949.

[6] T. Young, Philos. Trans. R. Soc. London **95**, 65 (1805).

[7] P.S. Laplace, *Celestial Mechanics*, Vol. IV [English translation of *Traité de Mécanique Céleste* IV (1805)] (Chelsea Publishing Company, Inc., New York, 1966).

[8] G. Hagen, Pogg. Ann. **46**, 423 (1839).

[9] J. Poiseuille, C. R. Acad. Sci. **11**, 961 (1840).

[10] O. Reynolds, Philos. Trans. R. Soc. London **174**, 935 (1883).

[11] J.M. Bell and F.K. Cameron, J. Phys. Chem. **10**, 658 (1906).

[12] G.D. West, Proc. R. Soc. London, Ser. A **86**, 20 (1911).

[13] H.E. Cude and G.A. Hulett, J. Am. Chem. Soc. **42**, 391 (1920).

[14] E.W. Washburn, Phys. Rev. **17**, 273 (1921).

[15] E.K. Rideal, Philos. Mag. **44**, 1152 (1921).

[16] L.R. Fisher and P.D. Lark, J. Colloid Interface Sci. **69**, 489 (1979).

[17] J.A. Mann, Jr., L. Romero, R.R. Rye, and F.G. Yost, Phys. Rev. E **52**, 3967 (1995).

[18] L.A. Romero and F.G. Yost, J. Fluid Mech. **322**, 109 (1996).

[19] R.R. Rye, J.A. Mann, Jr., and F.G. Yost, Langmuir **12**, 555 (1996).

[20] F.G. Yost, R.R. Rye, and J.A. Mann, Jr., Acta Mater. **45**, 5337 (1997).

[21] R.R. Rye, F.G. Yost, and E.J. O'Toole, Langmuir **14**, 3937 (1998).

[22] A.A. Darhuber, S.M. Troian, and W.W. Reisner, Phys. Rev. E **64**, 031603 (2001).

[23] *CRC Handbook of Chemistry and Physics*, 77$^{\rm th}$ *Edition* (CRC Press, Inc., Boca Raton, FL, 1996).

[24] Sigma-Aldrich Corp., St. Louis, MO (2002).

[25] Inland Vacuum Industries, Churchville, NY (2002).

[26] J.F. Douglas, *Introduction to Dimensional Analysis for Engineers* (Sir Issac Pitman and Sons, London, 1969).

[27] Note that normally the assumption for the pressure profile at $x \approx 0$ would be that Bernoulli's constant is conserved at the step. However, since the fluid velocities and dynamic pressures in these flows are quite low relative to the static pressure, we can neglect their contributions and assume continuity of static pressure at the step. This is shown rigorously in section V.

[28] Note that Fisher and Lark concluded that a velocity independent contact angle, θ, of $30^{\rm o}$ for water had to be assumed for agreement with the Washburn equation. We will not do this in our treatment, opting instead to use the typical water contact angle of $\theta = 0^{\rm o}$.

[29] Note that this correction differs from that proposed in Ref. [5]. The previously proposed correction would not allow R_{eff} to approach R as Bo approached 0.

[30] It is interesting to note that the similarity parameter, Π, is analogous to the Crocco number, Cr, of compressible gas dynamics[26], which is also equivalent to a velocity over a maximum velocity, V/V_{max}. In that case, V_{max} is the maximum velocity a gas can attain when adiabatically expanded to zero temperature.

[31] The worst departure can be attributed to large values of Bond number. At the highest values of Bo, it is likely that even our first-order correction discussed in Sect. IV D begins to fail.

[32] The implicit assumption in our introduction of the inviscid Bernoulli's equation is that the flow Reynolds number is low. The unsteady terms arising in the x-momentum equation as a result of using the inviscid Bernoulli's equation are not reliable except in their order of magnitude. However, we are only interested in the upper bound on these unsteady terms. The useful result of this derivation is the condition under which the neglect of the unsteady terms is justified.